Models-3 Community Multiscale Air Quality (CMAQ) model aerosol component 1. Model description

Francis S. Binkowski[1] and Shawn J. Roselle[1]

Atmospheric Sciences Modeling Division, Air Resources Laboratory, National Oceanic and Atmospheric Administration, Research Triangle Park, North Carolina, USA

Received 18 October 2001; revised 21 March 2002; accepted 16 December 2002; published 26 March 2003.

[1] The aerosol component of the Community Multiscale Air Quality (CMAQ) model is designed to be an efficient and economical depiction of aerosol dynamics in the atmosphere. The approach taken represents the particle size distribution as the superposition of three lognormal subdistributions, called modes. The processes of coagulation, particle growth by the addition of mass, and new particle formation, are included. Time stepping is done with analytical solutions to the differential equations for the conservation of number, surface area, and species mass. The component considers both PM2.5 and PM10 and includes estimates of the primary emissions of elemental and organic carbon, dust, and other species not further specified. Secondary species considered are sulfate, nitrate, ammonium, water, and secondary organics from precursors of anthropogenic and biogenic origin. Extinction of visible light by aerosols is represented by two methods: a parametric approximation to Mie extinction and an empirical approach based upon field data. The algorithms that simulate cloud interactions with aerosols are also described. Results from box model and three-dimensional simulations are exhibited. *INDEX TERMS:* 0305 Atmospheric Composition and Structure: Aerosols and particles (0345, 4801); 0345 Atmospheric Composition and Structure: Pollution—urban and regional (0305); 0365 Atmospheric Composition and Structure: Troposphere—composition and chemistry; 0368 Atmospheric Composition and Structure: Troposphere—constituent transport and chemistry; *KEYWORDS:* Models-3/CMAQ, PM, air quality modeling, visibility, aerosol species

Citation: Binkowski, F. S., and S. J. Roselle, Models-3 Community Multiscale Air Quality (CMAQ) model aerosol component, 1, Model description, *J. Geophys. Res.*, *108*(D6), 4183, doi:10.1029/2001JD001409, 2003.

1. Model Description

[2] The inclusion of aerosol particles in air quality models [*Seinfeld and Pandis*, 1998] may be done in several ways. Dividing the size range of the particle size distribution into a set of size sections has been very popular [*Gelbard et al.*, 1980; *Wexler et al.*, 1994; *Kleeman et al.*, 1997; *Meng et al.*, 1998; *Jacobson*, 1997, 1999]. Another method [*Wright et al.*, 2000] predicts the first six moments of the size distribution, but not the size distribution itself. The method chosen for the aerosol component of the CMAQ model [*Byun and Ching*, 1999] is derived from that introduced in the Regional Particulate Model (RPM) [*Binkowski and Shankar*, 1995], an extension of the Regional Acid Deposition Model (RADM) [*Chang et al.*, 1987, 1990]. As in RPM, a modal representation is assumed here. Fine particles with diameters less than 2.5 μm (PM2.5) are represented by two subdistributions or modes [*Whitby*, 1978] called the Aitken and accumulation modes. (Note: Aitken mode is used for the size range identified by Whitby as the "nuclei mode".) The Aitken mode includes particles with diameters up to approximately 0.1 μm for the mass distribution, and the accumulation mode covers the mass distribution in the range from 0.1 to 2.5 μm. *Whitby* [1978] also included a coarse mode. PM10 (particles with diameters less than 10 μm) mass is then represented by the sum of the masses in the Aitken, accumulation, and coarse modes.

[3] The modal representation has also been used by *Ackermann et al.* [1998], who applied a model similar to RPM to Europe. *Pirjola et al.* [1998] applied a monodisperse modal model to examine sulfate particle formation in the Arctic boundary layer.

[4] In the CMAQ modal approach one calculates only three integral properties of the size distribution for each mode: the total particle number concentration, the total surface area concentration, and the total mass concentration of the individual chemical components. The current approach differs from that taken by *Binkowski and Shankar* [1995] where the sixth moment was chosen as a third

[1]On assignment to National Exposure Research Laboratory, U.S. Environmental Protection Agency, Research Triangle Park, North Carolina, USA.

This paper is not subject to U.S. copyright.
Published in 2003 by the American Geophysical Union.

integral property, in place of the second moment. The sixth moment (the integral of the sixth power of the diameter over the size distribution) was chosen because of a mathematical simplification [see *Whitby and McMurry*, 1997] that allows analytical expressions to be used for the coagulation terms. The current approach uses Gauss-Hermite numerical quadratures [*Hildebrand*, 1974; *Davis and Rabinowitz*, 1967] to calculate all of the coagulation terms. This method is optimized for the mathematical form of the size distribution. The numerical quadratures used 10 points with the weights and abscissas taken from Table 25.10 of *Abramowitz and Stegun* [1965]. The numerical results were compared with the results from analytical expressions exhibited by *Whitby et al.* [1991], and are accurate to at least six decimal places. The choice of using numerical quadratures was made because the coagulation integral for second moment, unlike the sixth moment, does not have an analytical form.

[5] Conceptually within the fine group, the smaller Aitken (i) mode represents fresh particles either from nucleation or from direct emission, while the larger accumulation mode (j) mode represents aged particles. Primary emissions may also be distributed between these two modes. The two modes interact with each other through coagulation. Each mode may grow through condensation of gaseous precursors; each mode is subject to wet and dry deposition. Finally, the smaller mode may grow into the larger mode and partially merge with it. These processes are described in the following subsections. The chemical species treated in the aerosol component are fine sulfate, nitrate, ammonium, water, anthropogenic and biogenic organic carbon, elemental carbon, and other unspecified material of anthropogenic origin. The coarse-mode species are assumed to include sea salt (not yet implemented), wind-blown dust, and other as yet unspecified material of anthropogenic origin. Suppose atmospheric measurements of PM2.5 indicate the presence of species modeled in CMAQ as coarse mode species. How is this to be reconciled? The small particle tail of the coarse mode overlaps the range of the fine modes. A simple calculation using the error function at a diameter of 2.5 [μm] within the coarse will capture the fraction of such coarse material. The details of how the error function is related to the lognormal distribution are found on pp. 422 and 423 of *Seinfeld and Pandis* [1998].

[6] Most of the developmental work on the CMAQ aerosol component thus far has emphasized fine particulate matter, thus, the coarse mode has been implemented in a noninteractive way. That is, fine particles do not coagulate with coarse particles, nor do coarse particles coagulate with each other. This also means that dry deposition of chemical species that are emitted into the fine modes may be underestimated because a fractional amount of these species may have been moved to the coarse mode by intermodal coagulation where removal by particle dry deposition may be stronger. This process is ignored in the present implementation. We can estimate how significant this omission is by a simple calculation. Using the grand average continental size distribution given in Table 2 of *Whitby* [1978] with the Brownian coagulation algorithms described below, we estimated the following rates. For Number, the Aitken mode loses 31 [%/hr] by intramodal coagulation. The Aitken mode loses 72 [%/hr] to the accumulation mode and 0.1 [%/hr] to the coarse mode through intermodal coagulation. The values for the accumulation mode are 7 [%/hr] for intramodal losses and 0.008 [%/hr] for intermodal losses to the coarse mode. For surface area, the Aitken mode loses 8 [%/hr] by intramodal coagulation, and transfers 30 [%/hr] to the accumulation mode and 0.002 [%/hr] to the coarse mode by intermodal coagulation. The accumulation mode loses 0.8 [%/hr] by intramodal coagulation and transfers 0.002 [%/hr] to the coarse mode by intermodal coagulation. For Volume which is indicative of mass transfer, the Aitken mode transfers 21 [%/hr] to the accumulation mode and 0.02 [%/hr] to the coarse mode by intermodal coagulation. The accumulation mode transfers 0.0008 [%/hr] to the coarse mode by intermodal coagulation. This simple estimate of rates shows that for the grand average continental size distribution the interaction with the coarse mode is indeed weak. Future work, however, will include Brownian intermodal coagulation of Atken and accumulation modes with the coarse mode, as well as Brownian intramodal coagulation within the coarse mode.

[7] Finally, because atmospheric transparency, or visual range, is an important air quality related value, the aerosol component also calculates estimates of aerosol extinction coefficient and visual range using two methods (described below). Coarse mode particles are not included for the visual range calculations due to the large uncertainty in the estimate of emissions.

1.1. Aerosol Dynamics

[8] The particle dynamics of this aerosol distribution are described fully by *Whitby et al.* [1991] and *Whitby and McMurry* [1997]; therefore, only a brief summary of the method is given here. (Note: In the following equations repeated subscripts are not summed.)

[9] Given a lognormal distribution defined as

$$n(\ln D) = \frac{N}{\sqrt{2\pi}\ln\sigma_g}\exp\left[-0.5\left(\frac{\ln\frac{D}{D_g}}{\ln\sigma_g}\right)^2\right], \qquad (1)$$

where N is the particle number concentration (M_0) within the mode, D is the particle diameter, and D_g and σ_g are the geometric mean diameter and geometric standard deviation of the modal distribution, respectively. The k^{th} moment of the distribution is defined as

$$M_k = \int_{-\infty}^{\infty} D^k n(\ln D)\, d(\ln D) \qquad (2)$$

which after integration results in

$$M_k = N D_g^k \exp\left[\frac{k^2}{2}\ln^2\sigma_g\right]. \qquad (3)$$

M_0 is the number N of aerosol particles within the mode, suspended in a unit volume of air. For $k = 2$, the moment is proportional to the total particulate surface area within the mode, per unit volume of air. For $k = 3$, the moment is proportional to the total particulate volume within the mode, per unit volume of air. The constant of proportionality

Table 1. Aerosol Species[a]

	Abbreviation	Description
{a1}	ASO4J	Accumulation mode sulfate mass
{a2}	ASO4I	Aitken mode sulfate mass
{a3}	ANH4J	Accumulation mode ammonium mass
{a4}	ANH4I	Aitken mode ammonium mass
{a5}	ANO3J	Accumulation mode nitrate mass
{a6}	ANO3I	Aitken mode aerosol nitrate mass
{a7}	AORGAJ	Accumulation mode anthropogenic secondary organic mass
{a8}	AORGAI	Aitken mode anthropogenic secondary organic mass
{a9}	AORGPAJ	Accumulation mode primary organic mass
{a10}	AORGPAI	Aitken mode mode primary organic mass
{a11}	AORGBJ	Accumulation mode secondary biogenic organic mass
{a12}	AORGBI	Aitken mode biogenic secondary biogenic organic mass
{a13}	AECJ	Accumulation mode elemental carbon mass
{a14}	AECI	Aitken mode elemental carbon mass
{a15}	A25J	Accumulation mode unspecified anthropogenic mass
{a16}	A25I	Aitken mode unspecified anthropogenic mass
{a17}	ACORS	Coarse mode unspecified anthropogenic mass
{a18}	ASEAS	Coarse mode marine mass
{a19}	ASOIL	Coarse mode soil-derived mass
{a20}	NUMATKN	Aitken mode number
{a21}	NUMACC	Accumulation mode number
{a22}	NUMCOR	Coarse mode number
{a23}	SRFATKN	Aitken mode surface area
{a24}	SRFACC	Accumulation mode surface area
{a25}	AH2OJ	Accumulation mode water mass
{a26}	AH2OI	Aitken mode water mass

[a]Concentration units: mass [$\mu g\ m^{-3}$], number [m^{-3}].

between M_2 and surface area is π; the constant of proportionality between M_3 and volume is $\pi/6$. Note that the geometric standard deviation is the same no matter which moment is selected. M_3 is determined as follows from the fine aerosol species (including water) listed in Table 1:

$$M_{3i} = \sum_{n=1}^{n_{\max}} \frac{\varphi_{i,n}}{\frac{\pi}{6}\rho_n}. \tag{4a}$$

$$M_{3j} = \sum_{n=1}^{n_{\max}} \frac{\varphi_{j,n}}{\frac{\pi}{6}\rho_n}. \tag{4b}$$

where $\varphi_{i,n}$ and $\varphi_{j,n}$ are the species mass concentrations [$\mu g\ m^{-3}$], of the nth species in each mode; ρ_n is the average bulk density of the nth species. The third moment for the coarse mode is obtained in a similar manner. Given values of number, second and third moment concentrations, the geometric mean standard deviation and the geometric mean diameter for each mode are diagnosed from

$$\ln^2(\sigma_g) = \frac{1}{3}[\ln(M_0) + 2\ln(M_3) - \ln(M_2)] \tag{5a}$$

$$D_g^3 = \frac{M_3}{N \exp\left[\frac{9}{2}\ln^2 \sigma_g\right]}. \tag{5b}$$

The prediction equations for number, second moment and species mass are given in section 1.4.

1.2. New Particle Production by Nucleation

[10] In the work presented here only sulfuric acid is assumed to form new particles. *Kulmala et al.* [2000] argue that clusters of sulfuric acid undergo ternary nucleation with ammonia and water based upon results of *Korhonen et al.* [1999], who present such a ternary nucleation mechanism. Thus our predictions of new particle production are likely to be underestimates of true new particle production from ternary nucleation. No other species, for example, iodine, as suggested by *Hoffmann et al.* [2001] nor any other nucleation mechanisms, such as ionization, as suggested by *Yu and Turco* [2001] are considered in CMAQ at present. As a minimum, future work will include a parameterization of ternary nucleation when such a parameterization becomes available. Although the CMAQ model aerosol component currently allows a choice of two particle production mechanisms, those of *Harrington and Kreidenweis* [1998a, 1998b] and *Kulmala et al.* [1998], in the work presented here only the Harrington and Kreidenweis method was used. This method predicts the rate of increase of the particle number J (in number per unit volume per unit time) by the nucleation from sulfuric acid vapor using both the production rate of sulfuric acid vapor from gas-phase oxidation of sulfur dioxide by the hydroxyl radical and the resulting mixing ratio of sulfuric acid vapor. Future work with CMAQ will include using the *Kulmala et al.* [1998] method. In order to predict the rate of increase of new mass and new surface area (second moment), an assumption about particle size is necessary. Following work by *Weber et al.* [1997], it is assumed that the new particles are 3.5 nm in diameter. *Weber et al.* [1997] reported concentration measurements of particles which are in the size range 2.7 to 4 nm. For simplicity we have chosen 3.5 nm as a convenient representative diameter. We recognize that this is a gross simplification. New particles resulting from nucleation are very likely to be much smaller and grow to the 2.7 to 4 nm sizes by a combination of coagulation and condensation of species other than sulfate [*Kulmala et al.*, 2001]. Representing this process is beyond the scope of the present contribution.

[11] Using either of these methods, the production rate of new particle mass [$\mu g\ m^{-3}\ s^{-1}$] is then

$$\frac{d\,Mass}{dt} = \frac{\pi}{6}\rho d_{3.5}^3 J \tag{6a}$$

and that for number [$m^{-3}\ s^{-1}$] is

$$\frac{d\,Num}{dt} = J \tag{6b}$$

and that for surface area [$m^2\ m^{-3}\ s{-}^1$] is

$$\frac{d\,Surf}{dt} = \pi d_{3.5}^2 J, \tag{6c}$$

where $d_{3.5}$ is the diameter of the 3.5 nm particle and ρ is the density of the particle (assumed to be sulfuric acid) at ambient relative humidity [*Nair and Vohra*, 1975]. All results presented here use the method of *Harrington and Kreidenweis* [1998a, 1998b].

1.3. Primary Emissions

[12] The 1995 U.S. EPA emission inventory for PM2.5 and PM10 does not contain information about size distri-

bution or chemical speciation. In the CMAQ work reported here, the assumption is that the major part of PM2.5 particulate mass emissions are in the accumulation mode with a small fraction in the Aitken mode; (i.e. 99.9% of PM2.5 is assumed to be in the accumulation mode and the remaining fraction, 0.1%, is assigned to the Aitken mode). Sensitivity studies will be conducted to evaluate this assumption. In order to estimate the emissions rate for number and second moment from the mass emissions rate, an assumed mass size distribution is required. It is convenient to express the emission rate for number E_0 and that for second moment E_2 in terms of a total emissions rate for third moment. This is shown schematically as follows, where E_n is the mass emissions rate for species n and ρ_n is the density for that species

$$E_{3n} = \left(\frac{6}{\pi}\right)\left(\frac{E_n}{\rho_n}\right) \tag{7a}$$

$$E_0 = \frac{\sum_n E_{3n}}{D_{gv}^3 \exp\left(-\frac{9}{2}\ln^2 \sigma_g\right)} \tag{7b}$$

$$E_2 = \frac{\sum_n E_{3n}}{D_{gv} \exp\left(-\frac{1}{2}\ln^2 \sigma_g\right)}, \tag{7c}$$

where the sum is taken over all emitted species. Note also that the geometric mean diameter for mass or volume, D_{gv}, is given by $D_{gv} = D_g \exp(3 \ln^2 \sigma_g)$ from the Hatch-Choate relations for a lognormal distribution [*Hatch and Choate*, 1929].

[13] In (7b) and (7c), E_0 and E_2 schematically represent the emissions rates for the various modes. In section 1.4, the nomenclature used to represent the emissions rate for number for each of the three modes will be respectively, E_{0i}, E_{0j}, and E_{0cor}. Emissions for the second moments will be indicated in a similar manner.

[14] Based upon the near source observations reported by *Whitby* [1978], we have chosen values of 0.3 μm for the geometric mean mass diameter D_{gv} and 2.0 for the geometric standard deviation σ_g for the accumulation mode. The corresponding values for the Aitken mode are 0.03 μm and 1.7, and those for the coarse mode are 6 μm and 2.2.

[15] The emissions inventory used for this contribution estimates that 90% of PM10 is fugitive dust, and that 70% of this dust consists of PM2.5 particles. The paradigm adopted for the CMAQ model is that fugitive dust is a coarse mode phenomenon with a tail that overlaps the PM2.5 range. Therefore, 90% of PM10 emissions are assigned entirely to the coarse mode species ASOIL (see Table 1). Sulfate emissions are treated differently in this version of CMAQ than in RPM. In RPM, sulfate emissions were treated as particles and distributed between the Aitken and accumulation modes. In CMAQ, the photochemical module has sulfate emissions incorporated into the chemical solver. Thus, the production rate for sulfuric acid will include direct emissions of sulfate. This rate is passed from the photochemical module to the aerosol module. Assigning fractional amounts of emitted PM2.5 and PM10 to the specific species in Table 1 is a matter of ongoing discussions with those responsible for preparing the national emissions inventory.

1.4. Numerical Solvers

[16] The numerical solvers for the two fine particle modes have been modified from those in RPM, which followed from *Whitby et al.* [1991]. The major difference is that the RPM solvers linearized the quadratic term for intramodal coagulation in the equation for modal number concentration. The new solvers in CMAQ retain this quadratic term.

[17] The number concentrations for the Aitken and accumulation modes are denoted as N_i and N_j, respectively. Intramodal coagulation coefficients are functions only of the geometric mean diameters and geometric standard deviations for each mode and are denoted as F_{0ii} and F_{0jj}. Similarly, the intermodal coagulation coefficient for coagulation between the Aitken and accumulation modes is F_{0ij}. For simplicity the following coefficients are defined. For the Aitken mode:

$$a_i = F_{0ii}$$

$$b_i = N_j F_{0ij}$$

$$c_i = \frac{d\,Num}{dt} + E_{0i},$$

with $\frac{d\,Num}{dt}$ from (6b); and for the accumulation mode

$$a_j = F_{0jj}$$

$$c_j = E_{0j}.$$

The emission rates for number concentration are E_{0i} and E_{0j} and are set to values determined for each mode from (7b).

[18] We may now write for the particle number concentrations

$$\frac{\partial N_i}{\partial t} = c_i - a_i N_i^2 - b_i N_i \tag{8a}$$

$$\frac{\partial N_j}{\partial t} = c_j - a_j N_j^2. \tag{8b}$$

Equation (8a), a Riccati type equation, and equation (8b), a logistics type equation, have different analytical solutions depending upon whether c_i and c_j are zero or nonzero. These analytical solutions are used in the CMAQ solver with the coefficients being held constant over one model time step. In discussing the analytical solutions to (8a) and (8b) subscripts will be omitted for simplicity.

[19] The solution to equation (8a) for $c_i \neq 0$ is of the form

$$N(t) = \frac{r_1 + r_2 \gamma \exp(\delta t)}{a[1 + \gamma \exp(\delta t)]},$$

where

$$\delta = \left(b^2 + 4ac\right)^{\frac{1}{2}}$$

$$r_1 = \frac{2ac}{b+\delta}$$

$$r_2 = \frac{b+\delta}{2}$$

$$\gamma = -\left(\frac{r_1 - aN(t_0)}{r_2 - aN(t_0)}\right)$$

For $c_i = 0$, the solution to equation (8a) is of the form

$$N(t) = \frac{bN(t_0)\exp(-bt)}{b + aN(t_0)[1 - \exp(-bt)]}$$

The solution to equation (8b) when $c_j \neq 0$ is of the same form as that of equation (8a), except that $b = 0$. The solution to (8b) when $c_j = 0$ also, known as Smoluchowski's solution, is

$$N(t) = \frac{N(t_0)}{1 + aN(t_0)t}.$$

The equations for the prediction of second moment, M_2, in the Aitken and accumulation modes are both of the form

$$\frac{\partial M_2}{\partial t} = P_2 - L_2 M_2$$

with solutions of the form

$$M_2(t) = \frac{P_2}{L_2} + \left[M_2(t_0) - \frac{P_2}{L_2}\right]\exp(-L_2 t).$$

In these equations, production and loss of M_2 are denoted by P_2 and L_2, respectively. For the Aitken mode, P_2 includes the increase of M_2 by the following processes: new particle formation from (6c); condensational growth (see equation (7a) of *Binkowski and Shankar* [1995]); and primary emissions from (7c). L_2 for the Aitken mode includes both intermodal and intramodal coagulation. For the accumulation mode, P_2 includes M_2 transfer by intermodal coagulation, condensational growth (see equation (7b) of *Binkowski and Shankar* [1995]) and primary emissions from (7c). L_2 for the accumulation mode accounts for intramodal coagulation.

[20] It is important to note that the history variable in CMAQ is the modal surface area which, as already noted, is πM_2. For convenience, however, within the internal aerosol subroutines, M_2 is the variable of interest. Before returning to the main CMAQ routines, M_2 is multiplied by π. That is why species a23 and a24 in Table 1 are identified as modal surface areas. It is also important to note that the surface area predicted by CMAQ is the surface area for spherical particles and may not represent the true surface area available in nonspherical particles or in porous particles such as carbon soot. Empirical correction factors may be needed for use of CMAQ surface area predictions in certain applications.

[21] The equations for mass concentration of species n may be written as

$$\frac{\partial \varphi_{i,n}}{\partial t} = P_{i,n} - L_i \varphi_{i,n} \tag{9a}$$

$$\frac{\partial \varphi_{j,n}}{\partial t} = P_{j,n}, \tag{9b}$$

where

$$P_{i,n} = \varphi'_{i,n} + E_{i,n} + R_n \Omega_i$$

$$L_i = C_{3ij}/M_{3i}$$

$$P_{j,n} = E_{j,n} + R_n \Omega_j + L_i \varphi_{i,n}$$

with new mass from nucleation given by $\varphi'_{i,n} = \frac{d\,Mass}{dt}$ from equation (6a), when n denotes sulfate and is zero otherwise. $E_{i,n}$ and $E_{j,n}$ are the emission rates and R_n the gas-phase production rate for species n. The factors Ω_i and Ω_j defined by equations (A17) and (A18) of *Binkowski and Shankar* [1995] represent the fractional apportionment of condensing species. F_{3ij} is the coagulation coefficient for the third moment.

[22] Note that the loss of mass in (9a) is a gain of mass in (9b), representing mass transfer by intermodal coagulation. There is no such transfer of number in (8a) and (8b) because of the convention that when a smaller particle coagulates with a larger particle there is a loss of number from the population of smaller particles, but no gain of number in the population of larger particles. There is, however, a transfer of mass. Equation (9a) has an analytical solution, holding the coefficients constant for the time step, of the form:

$$\varphi_i^n(t) = \frac{P_i^n}{L_i} + \left[\varphi_i^n(t_0) - \frac{P_i^n}{L_i}\right]\exp(-L_i t).$$

The solutions to (9b) are obtained by Euler forward step for each species, once again holding the production terms constant over that time step.

[23] The equation for the prediction of coarse mode mass is

$$\frac{\partial \varphi_{cor,n}}{\partial t} = E_{cor,n}.$$

The solution is by an Euler forward step. The equation for number has a similar form because, as already noted, coagulation is currently ignored. The number equation is also solved with an Euler forward time step.

1.5. Mode Merging by Renaming

[24] In the work of *Binkowski and Shankar* [1995], the Aitken mode diameters grew over the simulation period to become as large as those in the accumulation mode. While this is probably true in nature, it violates the modeling paradigm that two modes of distinct size ranges must always exist. This phenomenon can be modeled by mode merging, as follows. The Aitken mode diameter approaches those of the accumulation mode by small increments over

any model time step when particle growth and nucleation are occurring. Thus, an algorithm is needed that transfers number, surface area, and mass concentration from the Aitken mode to the accumulation mode when the Aitken mode growth rate (including emissions) exceeds the accumulation mode growth rate (including emissions) and the number of particles in the accumulation mode is no larger than that in the Aitken mode.

[25] This algorithm is formulated as follows [*Binkowski et al.*, 1996]. The diameter of intersection D_{ij} between the Aitken and accumulation modal number distributions can be calculated exactly, because this same diameter appears in the realizations of (1) defining the number distribution in the Aitken and in the accumulation modes. The number concentration in each mode at this diameter must be the same, thus defining the intersection of the distribution curves. After some algebra, a quadratic equation can be solved for x_{num} (defined in equation (10a)). The fraction of the total number of Aitken mode particles greater than this diameter is easily calculated from the complementary error function

$$F_{num} = 0.5[\mathrm{erfc}(x_{num})], \tag{10a}$$

where $x_{num} = \frac{\ln(D_{ij}/D_{gi})}{\sqrt{2}\ln(\sigma_{gi})}$ and D_{gi} is the geometric mean diameter for the Aitken mode number distribution.

[26] The number concentration corresponding to these particles is transferred to the accumulation mode, a process denoted here as renaming the particles. A similar process is used to transfer mass (k = 3) concentration and surface area (k = 2) concentration from the Aitken to the accumulation mode using the complementary error function corresponding to the appropriate moment.

$$F_k = 0.5[\mathrm{erfc}(x_k)] \tag{10b}$$

where $x_k = x_{num} - \frac{k\ln(\sigma_{gi})}{\sqrt{2}}$. For numerical stability, the transfer of number, surface area, and mass is limited so that no more than one half of the Aitken mode mass may be transferred at any given time step. This is accomplished by requiring that $\frac{3\ln(\sigma_{gi})}{\sqrt{2}} \le x_{num}$. The fraction of the total number, surface area (k = 2), and mass (k = 3) remaining in the Aitken mode is calculated as

$$\Phi_{num} = 0.5[1 + \mathrm{erf}(x_{num})] \tag{10c}$$

$$\Phi_k = 0.5[1 + \mathrm{erf}(x_k)]. \tag{10d}$$

Using these fractions, Aitken and accumulation mode number and mass concentrations are updated as

$$N_j = N_j + F_{num}N_i \tag{11a}$$

$$\varphi_{j,n} = \varphi_{j,n} + F_3\varphi_{i,n} \tag{11b}$$

$$M_{2j} = M_{2j} + F_2M_{2i} \tag{11c}$$

$$N_i = \Phi_{num}N_i \tag{11d}$$

$$\varphi_{i,n} = \Phi_3\varphi_{i,n} \tag{11e}$$

$$M_{2i} = \Phi_2M_{2i}. \tag{11f}$$

This method of particle renaming is analogous to the procedure discussed by *Jacobson* [1997] where particles are reassigned in the moving center concept of a bin model. When the particles grow beyond the boundaries of their size bin, they are reassigned to a larger bin and averaged with the new bin.

1.6. Aerosol Dry Deposition

[27] The dry deposition rate of particle zeroth, second, and third moments to the Earth's surface provides the lower boundary condition for the vertical diffusion of aerosol number, surface area, and species mass, respectively. The method of doing this follows the RPM approach [*Binkowski and Shankar*, 1995], with the following exceptions. In RPM, total fine mass was deposited; in CMAQ the species mass in each mode is deposited separately, using the dry deposition velocity for the third moment. In CMAQ, the impaction term is omitted for the coarse mode particles in the moment dry deposition velocities. See *Binkowski and Shankar* [1995, equations (A25)–(A34)] for details.

1.7. Cloud Processing of Aerosols

[28] Clouds are formed when the relative humidity reaches a value at which existing aerosol particles are activated. That is, they pass through a potential barrier and grow rapidly from a few micrometers to several micrometers to become cloud droplets (i.e. nucleation). Soluble gases are then dissolved into the cloud droplets where aqueous-phase chemical equilibria and reactions occur. The attack on dissolved sulfur dioxide by hydrogen peroxide, methyl-hydrogen peroxide, peroxyacetic acid, ozone, and catalytic oxidation by iron and manganese [*Walcek and Taylor*, 1986] produces a dissolved sulfate species (oxidation of Sulfur (IV) to Sulfur (VI)). Because these processes are very complex in detail and occur at subgrid scale, most cloud modeling methods in mesoscale meteorological models and in air quality models use simplified parametric approaches to model the effect of clouds, rather than modeling the clouds directly. This approach was used in RADM and RPM and is applied in the current version of CMAQ.

[29] The assumptions for aerosol behavior in clouds are as follows:

1. The Aitken (*i*) mode forms interstitial aerosol which is scavenged by the cloud droplets. All three integral properties of the Aitken mode respond to in-cloud scavenging.
2. The accumulation (*j*) mode forms cloud condensation nuclei and thus is distributed as aerosol within the cloud water. Mass, surface area, and number in this mode may be lost through precipitation. Mass, but not number, is increased by in-cloud scavenging of the Aitken mode.
3. All new sulfate mass produced by aqueous production is added to the accumulation mode, but the number of accumulation mode particles is unchanged as is the geometric standard deviation, σ_g, of the accumulation mode processes [cf. *Leaitch*, 1996] for cumulus clouds.
4. The assumption that the accumulation mode σ_g is not changed during cloud processing means that the surface area of the accumulation mode is reconstructed from the new mass and new number in the accumulation mode at the end of the cloud lifetime using the initial value of σ_g.

5. The aerosol is mixed vertically by the same mechanisms mixing other species. The wet removal of aerosol is proportional to wet removal of sulfate. This follows from the assumption that all aerosol particles are internally mixed. Thus, if sulfate particles are removed by wet deposition, all other aerosol species are also removed at the same rate.

[30] The limitations of this approach are as follows: (1) The cloud process modules are similar to those of RPM and RADM with cloud droplet number concentrations N_c being modeled by an empirical fit to data from *Bower and Choularton* [1992]. (2) Cloud droplet size distributions are lognormal with σ_{gc} set to 1.2. Using the cloud liquid water content and the cloud droplet number concentration, the geometric mean cloud droplet diameter d_{gc} can be calculated.

[31] The mathematical approach begins with an extension [*Binkowski and Shankar*, 1994; *Shankar and Binkowski*, 1994] of *Slinn*'s [1974] two-step model as used by *Chaumerliac* [1984]. The in-cloud scavenging of interstitial Aitken mode number, surface area and mass concentration, y_{ak}, may be represented by

$$\frac{\partial y_{ak}}{\partial t} = -\alpha_c\, y_{ak} \tag{12}$$

with the solution

$$y_{ak}(t + \tau_{cld}) = y_{ak}(t)\exp(-\alpha_c \tau_{cld}), \tag{13}$$

where α_c is the attachment rate for interstitial aerosol concentrations of number ($k = 0$), surface area ($k = 2$), and mass ($k = 3$).The attachment rate is assumed to be held constant over the cloud lifetime τ_{cld}. The initial values $y_{ak}(0)$ are determined after cloud mixing.

[32] The cloud water aerosol concentration is represented by

$$\frac{\partial y_{ck}}{\partial t} = \delta_{k3}(\alpha_c y_{ak} + P) - \beta y_{ck} \text{ for } k \neq 2, \tag{14}$$

where β is the precipitation removal rate, and P is the production of new sulfate mass by aqueous chemistry. The Kronecker delta indicates that only mass ($k = 3$) is increased for the accumulation mode by chemical production and in-cloud scavenging.

[33] The attachment rate α_c, using the form recommended by *Pruppacher and Klett* [1978] and including an enhancement factor for the settling velocity of the cloud droplets v_c, is given by

$$\alpha_c = 2\pi m_{1c}\langle D\rangle\left(1 + 0.5\ Pe^{1/3}\right), \tag{15}$$

where the first moment of the cloud droplet distribution is

$$m_{1c} = N_c d_{gc}\exp\left[\frac{1}{2}\ln^2(\sigma_{gc})\right] \tag{16}$$

and

$$Pe = \frac{v_c d_{gc}}{\langle D\rangle} \text{ is a Peclet number.} \tag{17}$$

The polydisperse diffusivity is given by

$$\langle D\rangle = \left(\frac{kT}{3\pi\mu}\right)\left(\frac{M_2 + 2A\lambda M_1}{M_3}\right), \tag{18}$$

where M_k are the moments of the aerosol distribution, A = 1.246, λ is the mean free path, and μ is the dynamic viscosity [*Whitby et al.*, 1991].

[34] The precipitation removal rate is given by

$$\beta = \frac{1}{\tau_{cld}}\left(\frac{[\delta SO_4]_{wetdep}}{[SO_4]_{init} + [SO_4]_{scav} + [\delta SO_4]_{prod}}\right), \tag{19}$$

where τ_{cld} is the cloud lifetime, $[\delta SO_4]_{wetdep}$ is the change in sulfate concentration due to precipitation loss, $[SO_4]_{init}$ is the sulfate concentration at the beginning of the cloud lifetime, $[SO_4]_{scav}$ is the amount of sulfate added from in-cloud scavenging of Aitken mode sulfate, and $[\delta SO_4]_{prod}$ is the amount of new sulfate produced by aqueous chemistry.

1.8. Aerosol Chemistry

[35] The aerosol chemical species are listed in Table 1. The secondary species sulfate is produced by chemical reaction of hydroxyl radicals with sulfur dioxide to produce sulfuric acid that may condense on existing particles or nucleate to form new particles. Emissions of fresh primary sulfate are treated in the gas-phase chemistry component of CMAQ, and these contribute to the total change in sulfate from the chemistry component. This is a change from RPM where primary sulfate emissions were treated as a source of new mass and new particle number. Other inorganic species, such as ammonia and nitric acid, are equilibrated with the aerosols.

[36] An assumption of the model is that organics influence neither the water content nor the ionic strength of the aerosol particles; however, this assumption may not be valid for many atmospheric aerosols. Although much progress has been made [e.g., *Saxena et al.*, 1995; *Saxena and Hildemann*, 1996], sufficient basic data are not yet available to treat the system in a more complete and correct way. Over continental North America for PM2.5, sea salt and soil particles are not considered in the equilibria. Thus, for the current release of CMAQ, only the equilibrium of the sulfate, nitrate, ammonium and water system is considered. The equilibria and the associated constants are based upon *Kim et al.* [1993a] and are shown in Table 2.

[37] The aerosol water content is computed using the ZSR method [*Kim et al.*, 1993a] from

$$W = \sum_n \frac{M_n}{m_{n0}(a_w)}, \tag{20}$$

where W is the aerosol liquid water content [kg m^{-3}], M_n is the atmospheric concentration of the nth species [moles m^{-3}], and m_{n0} is the molality [moles kg^{-3}] of the nth species at a value of water activity (fractional relative humidity) of a_w. The values for molality as a function of water activity are calculated from laboratory data from *Giauque et al.* [1960], *Tang and Munkelwitz* [1994], and *Nair and Vohra* [1975]. The water content of sulfate aerosols depends strongly upon the ionic ratio of ammo-

Table 2. Equilibrium Relations and Constants[a]

Equilibrium Relation	Constant	K(298.15)	a	b	Units
$HSO_4^-(aq) \iff H^+(aq) + SO_4^{2-}(aq)$	$\frac{[H^+][SO_4^{2-}]\gamma_{H^+}\gamma_{SO_4^{2-}}}{[HSO_4^-]\gamma_{HSO_4^{2-}}}$	1.015E-02	8.85	25.14	mol/kg
$NH_3(g) \iff NH_3(aq)$	$\frac{[NH_3(aq)]\gamma_{NH_3}}{P_{NH_3}}$	57.639	13.79	−5.39	mol/kg atm
$NH_3(aq) + H_2O(aq) \iff NH_4^+(aq) + OH^-(aq)$	$\frac{[NH_4^+][OH^-]\gamma_{NH^+}\gamma_{OH^-}}{[NH_3(aq)]\gamma_{NH_3}a_w}$	1.805E-05	−1.50	26.92	mol/kg
$HNO_3(g) \iff H^+(aq) + NO_3^-(aq)$	$\frac{[H^+][NO_3^-]\gamma_{H^+}\gamma_{NO_3^-}}{P_{HNO_3}}$	2.511E06	29.17	16.83	mol^2/kg^2 atm
$NH_4NO_3(s) \iff NH_3(g) + HNO_3(g)$	$P_{NH_3}P_{HNO_3}$	5.746E-17[b]	−74.38[b]	6.12[b]	atm^2
$H_2O(aq) \iff H^+(aq) + OH^-(aq)$	$\frac{[H^+][OH^-]\gamma_{H^+}\gamma_{OH^-}}{a_w}$	1.010E-14	−22.52	26.92	mol^2/kg^2

[a]From *Kim et al.* [1993a]. The constants a and b are used in the following to adjust for ambient temperature: $K = K(T_0)\exp\left[a\left(\frac{T_0}{T}-1\right)+b\left(1+\ln\left(\frac{T_0}{T}\right)-\frac{T_0}{T}\right)\right]$, $T_0 = 298.15[K]$.

[b]These values are only used by *Kim et al.* [1993a, 1993b]. The values used in the CMAQ model are from *Mozurkewich* [1993]: $K = \exp\left(118.87 - \frac{24084}{T} - 6.025\ln(T)\right)$, where Mozurkewich reports in nanobars squared. This yields a value for the equilibrium constant of 43.11 $[nb^2]$ at 298.15 K.

nium to sulfate. This ratio varies from zero for sulfuric acid to 2.0 for ammonium sulfate with intermediate values of 1.0 for ammonium bisulfate, and 1.5 for letovicite. The usual method of applying the ZSR method would span this range with a single expression; however, *Spann and Richardson* [1985] have shown that this is not correct. They proposed a modification which resulted in a correction term. A very similar result is obtained by using the ZSR method between the ranges of the ionic ratio of sulfuric acid to ammonium bisulfate, ammonium bisulfate to letovicite, and letovicite to ammonium sulfate. The binary activity coefficients are computed using Pitzer's method and the Bromley method is used for the multicomponent activity coefficients in the aqueous solution (see *Kim et al.* [1993a] for details).

[38] Two regimes of ammonium to sulfate ionic ratio are considered. The ammonia deficient regime (in which the ionic ratio of ammonium to total sulfate ion is less than 2.0) leads to an acidic aerosol system with very low concentrations of dissolved nitrate ion which depend very strongly on ambient relative humidity. The second regime is one in which the ammonium to sulfate ratio exceeds 2.0, the sulfate is completely neutralized, and there is excess ammonia. If there is nitric acid vapor in the system, it will dissolve in the aqueous particles along with the excess ammonia and produce abundant nitrate.

[39] For cases when the relative humidity is so low that the aerosol liquid water content comprises less than 20 percent of the total aerosol mass, and the ionic ratio of ammonium to sulfate is greater than 2.0, ''dry ammonium nitrate'' aerosol is calculated with the following equilibrium relationship:

$$NH_4NO_3(s) \Leftrightarrow NH_3(g) + HNO_3(g). \quad (21)$$

The value of the equilibrium constant is taken from *Mozurkewich* [1993] as noted in Table 2.

[40] Precursors of anthropogenic organic aerosol (such as alkanes, alkenes, and aromatics) react with hydroxyl radicals, ozone, and nitrate radicals to produce condensable material. Monoterpenes react in a similar manner to produce biogenic organic aerosol species. The rates of production of sulfuric acid and the organic species are passed from the photochemical component of CMAQ to the aerosol component. The formation rates of aerosol mass (in terms of the reaction rates of the precursors) are taken from *Pandis et al.* [1992]. These factors are given in Table 3. *Zhang et al.* [2000] have evaluated the inorganic equilibrium model described here.

1.9. Visual Range

[41] Visibility is usually defined to mean the furthest distance one both can see and identify an object in the atmosphere. For a detailed presentation on the concepts of visibility, see *Malm* [1979]. In a perfectly clean atmosphere composed only of nonabsorbent gases, the only process restricting visibility during daylight is the scattering of solar radiation from the gas molecules. This is known as Rayleigh scattering, usually represented by a scattering coefficient. If absorption is also occurring in addition to scattering, an absorption coefficient may also be defined. The sum of the scattering and absorption coefficients is called the extinction coefficient. If absorption is not occurring, the extinction coefficient is equal to the scattering coefficient. The visibility in an atmosphere in which Rayleigh scattering is the only active optical process may be taken as a reference. A useful index for quantifying the impairment of visibility by the presence of atmospheric aerosol particles is the deciview

Table 3. Organic Aerosol Yields in Terms of Amount of Precursor Reacted[a]

Gas-Phase Organic Species	Aerosol Yield, $\mu g\ m^{-3}$/ppm (Reacted)
C8 and higher alkanes	380
anthropogenic internal alkenes	247
monoterpenes	740
toluene	424
xylene	342
cresol	221

[a]From *Pandis et al.* [1992] and *Bowman et al.* [1995].

[*Pitchford and Malm*, 1994]. The deciview index, *deciV*, is given as

$$deciV = 10 \ln\left(\frac{\beta_{ext}}{0.01}\right) \tag{22}$$

with $\beta_{ext} = \beta_{sp} + 0.01$ [km^{-1}] where 0.01 is the standard value for Rayleigh extinction.

[42] The aerosol extinction coefficient β_{sp} [km^{-1}] must be calculated from such ambient aerosol characteristics as index of refraction, volume concentration and size distribution; at wavelength λ,β_{sp} may be expressed as

$$\beta_{sp} = \frac{3\pi}{2\lambda} \int_{-\infty}^{\infty} \frac{Q_{ext}}{\alpha} \frac{dV}{d\ln\alpha} d\ln\alpha, \tag{23}$$

where the particle distribution is given in a lognormal form as

$$\frac{dV}{d\ln\alpha} = V_T \left(\frac{A}{\pi}\right)^{1/2} \exp\left[-A \ln^2\left(\frac{\alpha}{\alpha_v}\right)\right], \tag{24}$$

where $\alpha = \frac{\pi D}{\lambda}$ and $\alpha_v = \frac{\pi D_g}{\lambda}$ and $A = \frac{1}{2\ln^2 \sigma_g}$. V_T is the total particle volume concentration, and Q_{ext}, the Mie extinction efficiency factor, is a function of α and the index of refraction of the particles. *Willeke and Brockmann* [1977] showed that the behavior of the extinction coefficient is a smooth function of the geometric mean diameter for the volume distribution D_{gv} and the index of refraction. This smooth characteristic implies that an accurate approximation to the Mie efficiency can be used in its place to reduce a very computationally intensive task. The method of *Evans and Fournier* [1990], a highly accurate approximation, is used to calculate Q_{ext}.

[43] Because routine measurements of aerosol species mass concentrations are often available, but particle size distribution information is not, an additional method of calculating extinction has also been included. This is an empirical approach known as "reconstructed mass extinction". The method is explained by *Malm et al.* [1994]. The formula used here is a slight modification of their equation (12) (J. Sisler, personal communication, 1998). The aerosol extinction coefficient β_{sp}, is given by

$$\begin{aligned}\beta_{sp}[1/\mathrm{km}] = {} & 0.003*\mathrm{f(RH)}*\{[\text{ammonium sulfate}] \\ & +[\text{ammonium nitrate}]\} + 0.004*[\text{organic mass}] \\ & + 0.01*[\text{Light AbsorbingCarbon}] \\ & + 0.001*[\text{fine soil}] + 0.0006*[\text{coarse mass}].\end{aligned} \tag{25}$$

In implementing the above equation, the term in braces is determined by adding ammonium plus sulfate plus nitrate. Organic mass is taken as the sum of all organic species. Light absorbing carbon is elemental carbon. Fine soil is taken as the unspeciated portion of PM2.5 emitted species, and the coarse mass term is not currently implemented in CMAQ system because uncertainty in the emissions is too large. The relative humidity correction, f(RH), is obtained from a look-up table of corrections given in *Malm et al.* [1994].

Table 4. Box Model Inputs

	Clear Case	Urban Case	Hazy Case
NUMATKN [m^{-3}]	1.255668e9	1.037999e11	2.343418e9
ASO4I [$\mu g\ m^{-3}$]	0.054	1.134	0.162
SRFATKN [$m^2\ m^{-3}$]	3.565694e-6	1.182309e-4	1.247841e-5
NUMACC [m^{-3}]	6.451020e8	3.227957e10	3.793163e9
ASO4J [$\mu g\ m^{-3}$]	1.8	69.12	10.44
SRFACC [$m^2\ m^{-3}$]	3.350347e-5	9.685348e-4	1.723419e-4
NUMCOR [m^{-3}]	7.2519e5	5.2103e6	3.7565e6
ACORS [$\mu g\ m^{-3}$]	7.2519e5	67.76	56.98

2. Box Model Simulations

[44] In order to provide a test of confidence of the aerosol dynamics algorithms, a box model test version of the CMAQ aerosol component that includes all of the processes already described was developed. The box model was then used for three cases that have been discussed in the literature [*Seigneur et al.*, 1986; *Zhang et al.*, 1999; *Fernández Díaz et al.*, 1998]. The three cases are identified as Clear, Urban, and Hazy. The Clear and Urban cases are tests of coagulation under low and high particle concentrations, respectively. The Hazy case is a test of strong condensational growth. The cases were run for 12 hours with a 600-second time step. The input values for the cases are listed in Table 4. Figure 1 displays the results from the Clear case. Figure 1a shows that even in a case with such a small number concentration, coagulation was important in changing the Aitken mode number distribution; the volume distribution (Figure 1b) and the surface area distribution (Figure 1c) are little affected by coagulation. The situation is very different in the Urban case. Figure 2a shows that the Aitken mode number distribution responds very strongly to coagulation, as do the volume (Figure 2b) and surface area (Figure 2c) distributions. *Zhang et al.* [1999], following the arguments of *Seigneur et al.* [1986], see the change in the volume distribution as an error arising from the use of a lognormal rather than a sectional model. The view taken here is that applying the sectional model to either volume (mass) or number independently does not provide a complete representation of aerosol dynamics. Starting with an initial lognormal distribution and using a sectional mode for number as shown by *Zhang et al.* [1999], results in a distribution seen to be skewed and not lognormal. However, real atmospheric particles appear to be lognormal as shown, for example, by *Mäkelä et al.* [2000]. The CMAQ modal approach treats number, surface area, and volume (mass) in a consistent, coupled approach using analytical solutions to the governing differential equations.

[45] Turning to the results for the Hazy case shown in Figure 3, we see that the distribution for each of the moments shows a strong modal separation between the Aitken and accumulation modes. The version of CMAQ discussed by *Zhang et al.* [1999] did not show this behavior. That version assumed that the geometric standard deviation did not vary from an initial value in either the Aitken or accumulation modes. Figure 4 shows the same results of Figure 3b plotted with the high resolution sectional model that was denoted as "exact" results shown by *Zhang et al.*

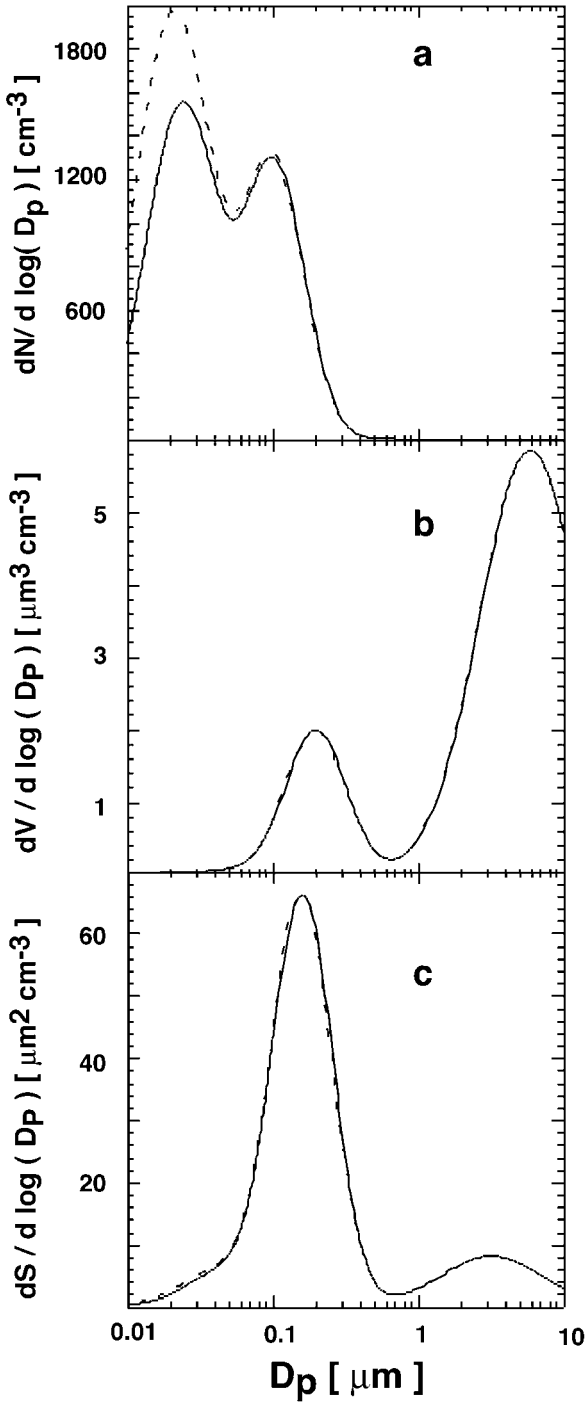

Figure 1. Size distributions for the *Seigneur et al.* [1986] Clear case. (a) Number concentration distribution, (b) volume concentration distribution, (c) surface area concentration distribution. Values are shown for the initial time (t = 0) as a dashed curve and the final time (t = 12 hours) as a solid curve.

[1999]. The peak of the Aitken mode aligns with that of the AER "exact" simulation, but at a slightly larger diameter. The peak of the accumulation mode is aligned with the initial value, and exceeds that of the AER "exact" simulation presumably because of coagulation (as observed in the Urban case). The peak of the accumulation mode in the "exact" simulation is shifted to a smaller diameter. This phenomenon is also present in the simulations of *Fernández Díaz et al.* [1998]; note also that the amplitude of the Aitken mode peak in their simulation has a larger amplitude than either that in the CMAQ or "exact" simulations.

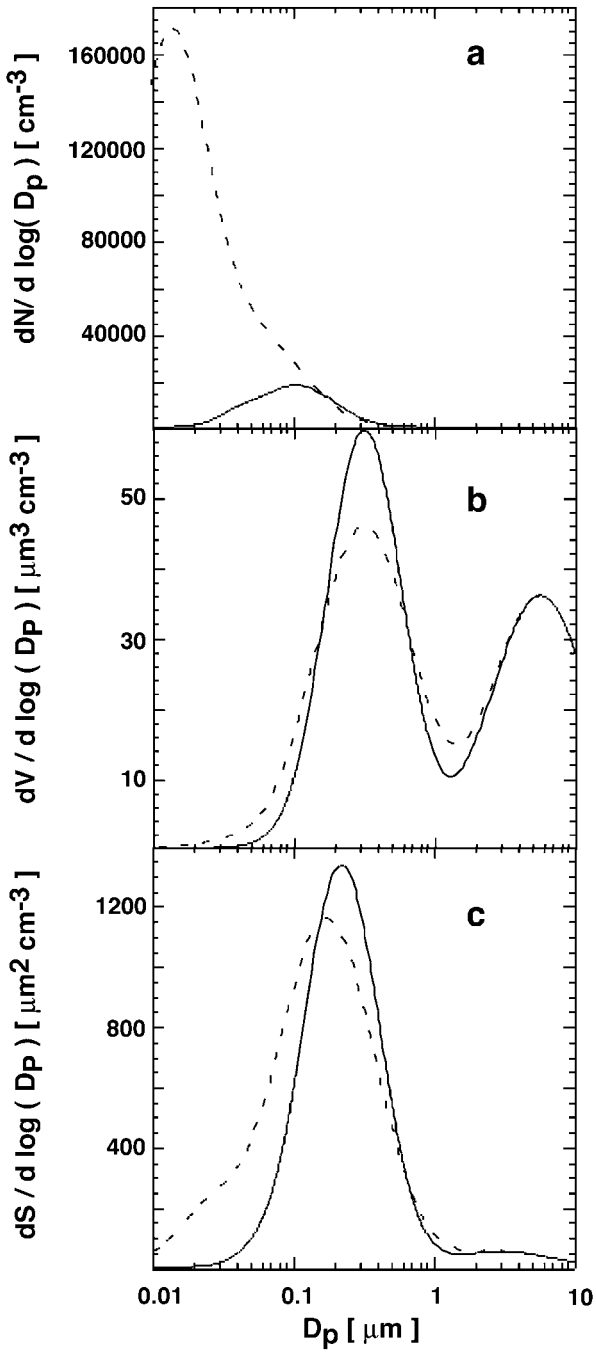

Figure 2. Size distributions for the *Seigneur et al.* [1986] Urban case. (a) Number concentration distribution, (b) volume concentration distribution, (c) surface area concentration distribution. Values are shown for the initial time (t = 0) as a dashed curve and the final time (t = 12 hours) as a solid curve.

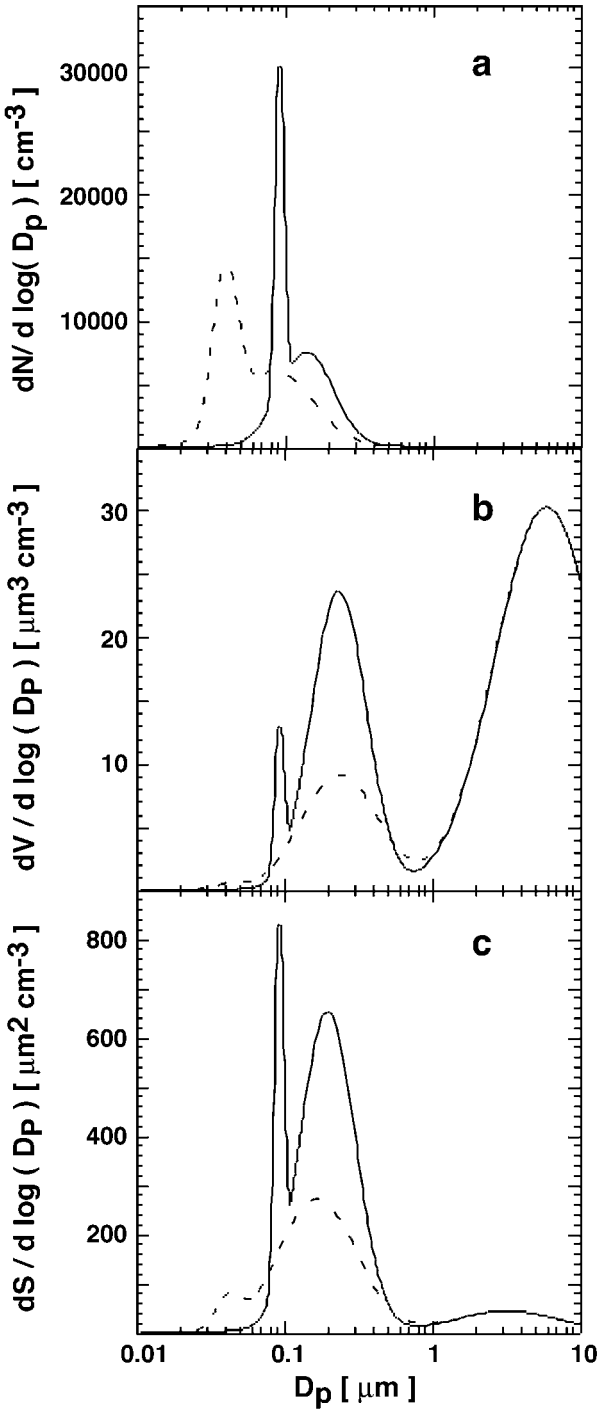

Figure 3. Size distributions for the *Seigneur et al.* [1986] Hazy case. (a) Number concentration distribution, (b) volume concentration distribution, (c) surface area concentration distribution. Values are shown for the initial time (t = 0) as a dashed curve and the final time (t = 12 hours) as a solid curve.

[46] The simulations of *Zhang et al.* [1999] and *Fernández Díaz et al.* [1998] considered only condensation and ignored the possibility of coagulation in the hazy case. The simulation done by *Zhang et al.* [1999] with the older CMAQ model was performed without coagulation with their "Models-3 (AER)" version. As already noted, all simulations done here are with the full aerosol dynamics active (i.e., condensational growth and coagulation active). It is not clear whether this is a complete explanation of the differences between the CMAQ and "exact" results or whether this difference is an inherent artifact of the modal approach. It would be interesting to see the simulations of the hazy case done with a high resolution sectional model which includes both condensation and coagulation.

3. Transport Issues

[47] Implementing the aerosol component into a three-dimensional Eulerian model like CMAQ required some care regarding exactly how the modal distribution moments and masses would be transported. The basic hypothesis of the approach is that the mathematical form of the size distribution remains lognormal. Thus, at the end of a transport step, the moments are always reassembled into lognormal distributions. Transport by the wind (advection) and by turbulent diffusion within an Eulerian model may be viewed as a process of mixing values from one grid cell with those of a second grid cell. The matter is well understood with scalars, such as the mixing ratios of trace gases. In a sectional model, this analogy is carried forth with the mass concentrations in the various sections being advected or diffused [*Jacobson*, 1999]. In a modal model, the issue is not so easily understood. For example, in modeling vertical diffusion in the well-mixed planetary boundary layer (PBL), potential temperature and water vapor mixing ratio are nearly constant. Temperature and relative humidity are, of course, not constant. At the higher altitudes within the PBL, aerosol particles may have more liquid water than those at the lower altitudes. Within the CMAQ, adjustment to

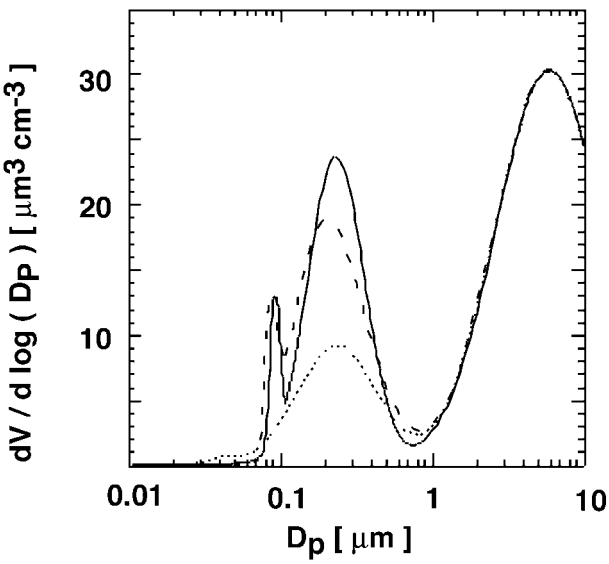

Figure 4. Comparison of CMAQ volume concentration size distribution (solid curve) with the "exact" distribution (dashed curve) of *Zhang et al.* [1999]. The initial values are shown by the dotted curve. The CMAQ curve is the same as shown in Figure 3b.

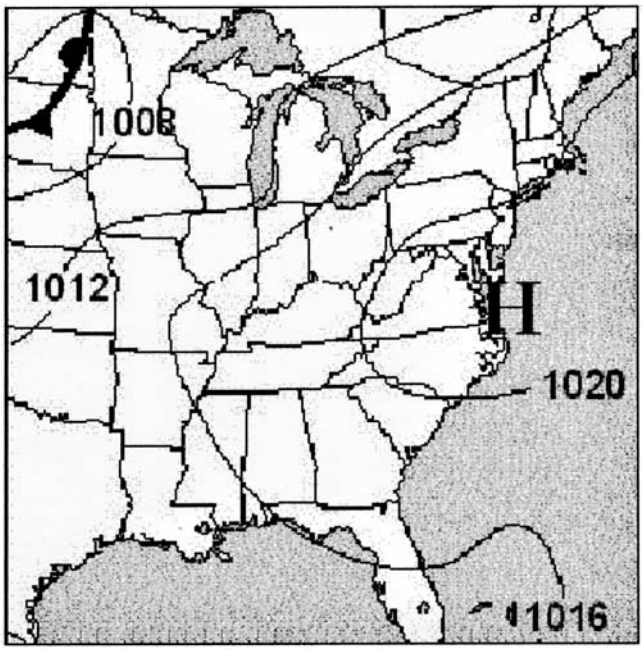

Figure 5. Surface weather map for 12Z on July 13, 1995.

relative humidity is done by keeping the geometric standard deviation unchanged. This is a reasonable approximation if saturation does not occur. If, however, one mixes the "more wet" particles aloft, with "less wet" particles from below it is easy to show that this process increases the geometric standard deviation, changing the underlying size distribution of "dry particles", which should be unchanged in a well mixed PBL. Various numerical sensitivity studies with CMAQ confirm this. The same arguments made for the vertical diffusion hold for advection when there is a sharp gradient in water vapor. Therefore, all transport is done assuming the particles are "dry" and equilibration with water vapor is done after transport, but before any aerosol dynamics calculations are done. This is accomplished as follows. Number and species mass other than water are the same in "wet" and "dry" particles. The adjustment really only affects the surface area. Particles which have grown by acquiring liquid water have a larger surface area. Then the surface area must be set to that of particles without the liquid water. To adjust these particles for transport, the assumptions are that the number concentration and the geometric standard deviation are unchanged after removing the liquid water from the particles. Then the following is a valid method of adjusting the surface area for each mode. Starting with the second and third moments as defined, determine their natural logarithms, and then form a perturbation in the moments. Because the geometric mean standard deviations of the moments are the same, the second moment responds to the changed values of the third moment as

$$M_2^d = M_2^w \left(\frac{M_3^d}{M_3^w} \right)^{2/3},$$

where the superscripts w and d refer to the "wet" and "dry" particles, respectively. Multiplication of the resulting second moment by π then yields the new surface area for the mode. This method then assures that the problem described in transporting the moments is eliminated.

4. Results for a Three-Dimensional CMAQ Simulation

[48] Results are displayed for 17Z on July 13, 1995, from a 3-D CMAQ simulation covering the eastern United States for the period from 00Z on July 11, 1995 until 00Z on July 16, 1995. This time period consists of the last 120 hours of a 239-hour simulation that began at 00Z on July 6, 1995, and was done in 24-hour segments. The computational grid has a horizontal resolution of 36 km and extends in the vertical to an altitude of approximately 16km (equivalent to a pressure of 10 kPa). All results presented here are for the lowest layer, which is 40 m thick. The simulation was done with the Carbon Bond (CBIV) [*Gery et al.*, 1989] mechanism, which was extended to allow for production of secondary organic aerosol (SOA) material from anthropogenic and biogenic precursors. The *Pandis et al.* [1992] method was applied for production of SOA from aromatics (anthropogenic) and from monoterpenes (biogenic) assumed to be alpha pinene. Figure 5 shows the weather map for 12Z on July 13, 1995. During this 120-hour simulation period, a large anticyclone dominated the circulation over the eastern United States.

[49] Spatial plots of various aerosol mass concentrations at 17Z on July 13, 1995 are shown in Figures 6 through 10. Figure 6 shows the PM2.5 mass concentration. Note that as is the practice for reporting particulate matter (PM) measurements, the contribution of water has been omitted. The broad maximum extending from the confluence of the Ohio and Mississippi Rivers through southern Indiana into western Ohio is dominated by aerosol sulfate, as is seen in Figure 7, where the contribution of sulfate in this area is

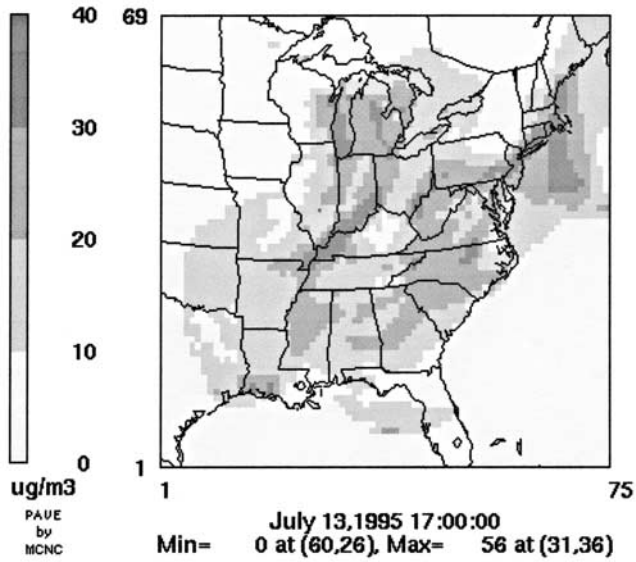

Figure 6. Total PM2.5 mass concentration predicted by CMAQ for 17Z on July 13, 1995. All Aitken and accumulation mode species except aerosol water are included.

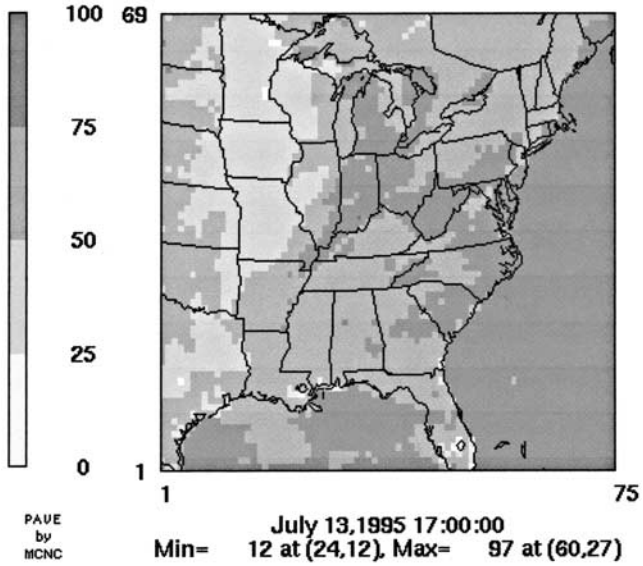

Figure 7. The percent contribution of aerosol sulfate (ASO4I + ASO4J) to PM2.5 mass concentration at 17Z on July 13, 1995.

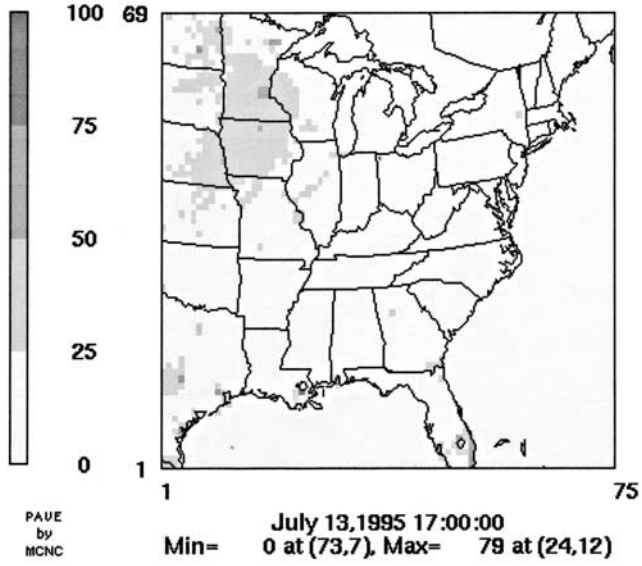

Figure 9. The percent contribution of primary species (AORGPAI + AORGPAJ + AECI + AECJ + A25I + A25J) to PM2.5 mass concentration at 17Z on July 13, 1995.

greater than 75%. Over the Atlantic, sulfate is over 90% of the PM2.5 mass, although the concentrations are less than 10 $\mu g\ m^{-3}$. Ammonium contributes 20% or more over the Midwest (Figure 8). The molar ratio of ammonium to sulfate (not shown) is 2.0 or greater over nearly the same region, indicating that the sulfate is fully neutralized. Note that in comparing Figure 8 with Figure 7, a minimum in ammonium over West Virginia and eastern Pennsylvania corresponds to a maximum in sulfate over the same area. One would then expect the aerosol particles in this area to be acidic. The maximum contribution from primary emissions (the sum of primary organic carbon, elemental carbon, and other unspecified material) shown in Figure 9 has a maximum in southern Louisiana. A cautionary note must be sounded in that the emission inventory for PM2.5 is being updated for 1996 and subsequent years and the results presented here for primary species will be subject to revision. The contribution to the coarse mode (Figure 10) is also from primary emissions only. The maximum shown is in southern Texas, near Houston. The same caveats as made for PM2.5 hold for the coarse mode.

[50] As seen in Figures 6–10, results from the CMAQ aerosol component appear to be plausible. Careful evaluation against observational data is necessary. A preliminary

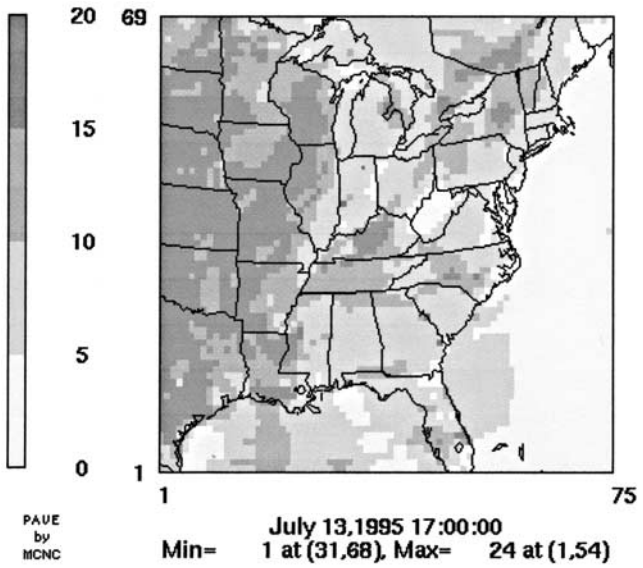

Figure 8. The percent contribution of aerosol ammonium (ANH4I + ANH4J) to PM2.5 mass concentration at 17Z on July 13, 1995.

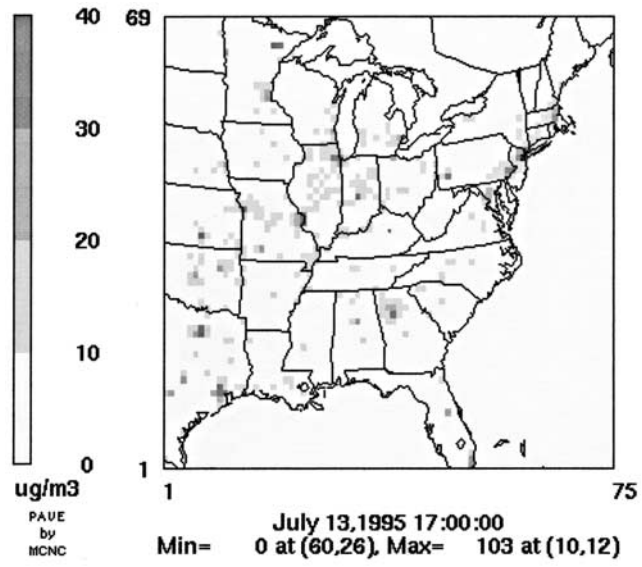

Figure 10. Total coarse mode mass concentration (ACORS + ASOIL) at 17Z on July 13, 1995. Note that sea salt (ASEAS) is not active in this simulation.

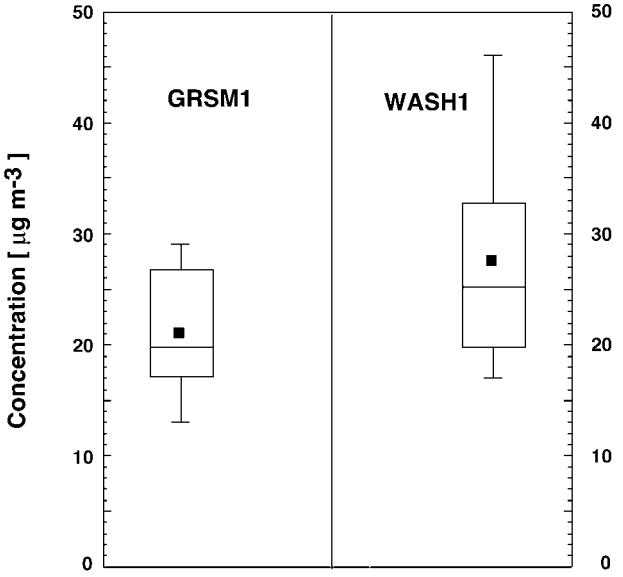

Figure 11. Box plots of PM2.5 mass concentration for the 120-hour simulation from 00Z on July 11, 1995 to 00Z on July 15, 1995. Values for selected grid cells are shown. See text for identity of the grid cells.

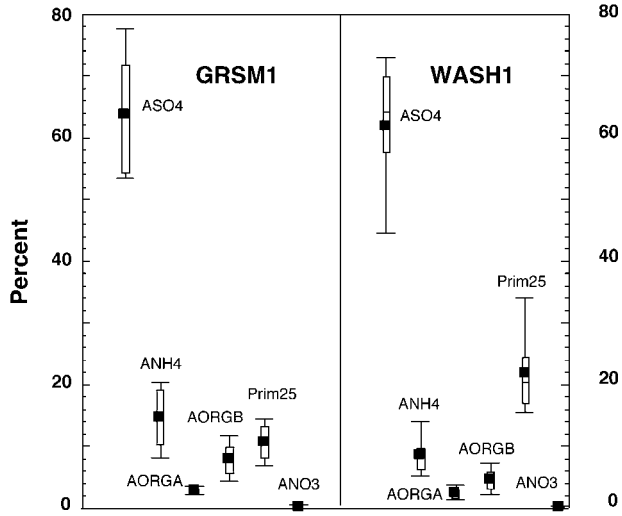

Figure 12. Box plots for the percent contribution to the PM2.5 concentrations shown in Figure 11. The species represented are sums of the Aitken and accumulation mode contributions. Prim25 is as defined in Figure 9.

evaluation will be presented in a companion paper by *Mebust et al.* [2003].

5. Statistical Results From Two Selected Grid Cells

[51] Model simulation results from two grid cells were selected for further analysis. The grid cell containing the Great Smoky Mountain National Park in western North Carolina and eastern Tennessee was selected as representative of a rural location. The identifier GRSM1 is used for this grid cell. The grid cell containing Washington, D. C., was selected as representing an eastern urban to suburban location. The identifier WASH1 is used for this grid cell. The identifiers are those of the IMPROVE network observing sites located within each grid cell and will be discussed further by *Mebust et al.* [2003]. Model output covering the entire 120-hour simulation period will be presented as box plots. Such plots show the range of values as follows. The 90th and 10th percentiles are shown as whiskers at the top and bottom of the box, respectively. The 75th percentile and 25th percentiles are the top and bottom of the main box, respectively. The box is divided into two parts by a line showing the 50th percentile, and the mean value is displayed as a dark square in the box. 11 shows box plots for the simulated PM2.5 concentrations at GRSM1 and WASH1. The range of modeled concentration values is much larger in the WASH1 grid cell than in the GRSM1 grid cell, and the mean and median have larger values in the WASH1 grid cell. The contributions from the various species (Figure 12) show that for the two selected grid cells, sulfate is the dominant species. Primaries (emitted species) are more important than other species only for the WASH1 grid cell. For the GRSM1 grid cell, ammonium is the second most important species. As would be expected, SOA of biogenic origin is much more important in the GRSM1 grid cell than in the WASH1 grid cell. A strong caveat is in order for these SOA species. Their contributions should be taken as crude estimates only. This simulation used the fractional aerosol coefficient approach of *Pandis et al.* [1992]. *Schell et al.* [2001] have shown how the partitioning approach of *Odum et al.* [1996] can be included in a comprehensive air quality model. This partitioning method of accounting for SOA is now the preferred method and will be included in the next version of CMAQ.

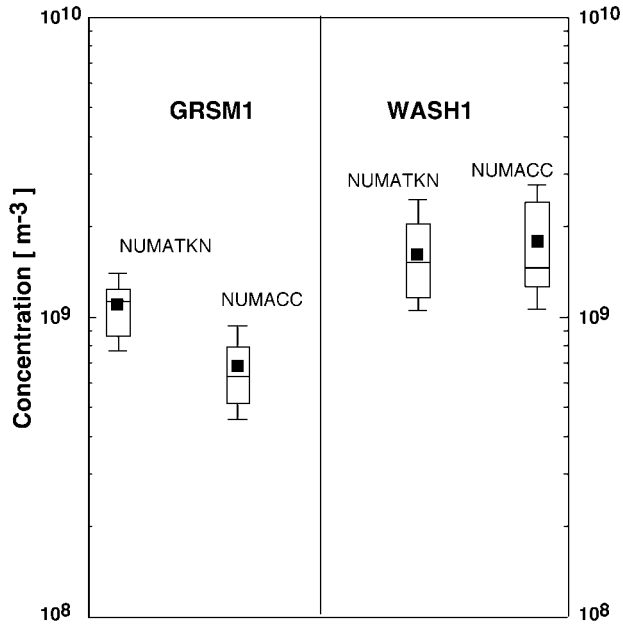

Figure 13. Box plots for the modal number concentration in the Aitken and accumulation modes for the selected grid cells.

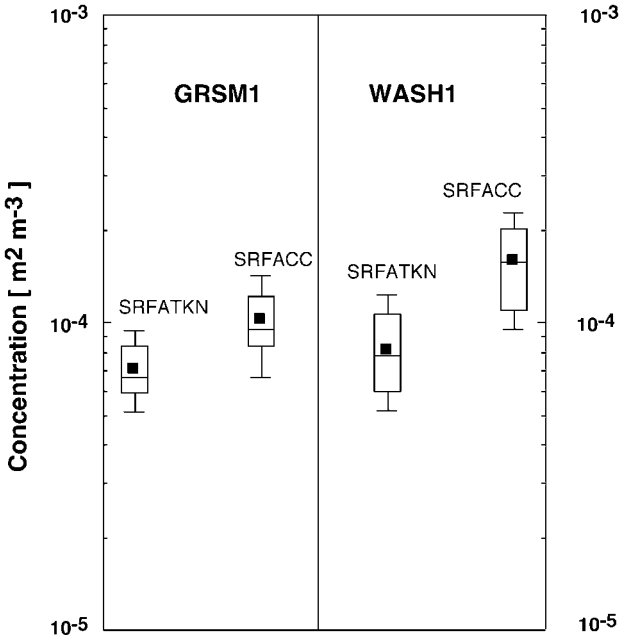

Figure 14. Box plots for the modal surface area concentration in the Aitken and accumulation modes for the selected grid cells.

[52] In Figures 13 and 14 we see the behavior of number and "dry" surface area concentrations, respectively. The WASH1 grid cell has a higher number concentration than the GRSM1 grid cell, especially in the accumulation mode. This grid cell also has the higher surface area concentration for the accumulation mode. It appears that this is due to the greater contribution of the primary emissions.

[53] Figures 15 and 16 for 17Z on July 13, 1995, show how the size distributions change when water is considered. The curves marked "wet" include aerosol water; those marked "dry" do not. The "dry curves" may be thought of as resulting from a virtual dryer applied to the size distributions, removing the water, but nothing else. All aerosol dynamics calculations previously described are done on the "wet" distributions. As already noted, the surface area is adjusted to the "dry" value for transport.

[54] Note that all of these analyses are performed on values from model simulations, not observed data. These two grid cells contain the locations of the IMPROVE network particle measuring sites. Data from these sites will be used in a companion paper for evaluation of CMAQ model estimates [*Mebust et al.*, 2003].

6. Summary

[55] The CMAQ aerosol component is a major extension of the RPM. Addition of the coarse mode and primary emissions now allow both PM2.5 and PM10 to be modeled. As already noted, future versions will include the intermodal coagulation between the Aitken and accumulation modes and the coarse mode. Work already in progress will improve the representation of the production of SOA material by including a version of the method of *Pankow* [1994a, 1994b] as discussed by *Odum et al.* [1996]. This method, based upon laboratory experiments, calculates the yield of SOA as a function of the amount of organic material already in the particle phase. *Schell et al.* [2001] have shown how this approach can be applied in a three-

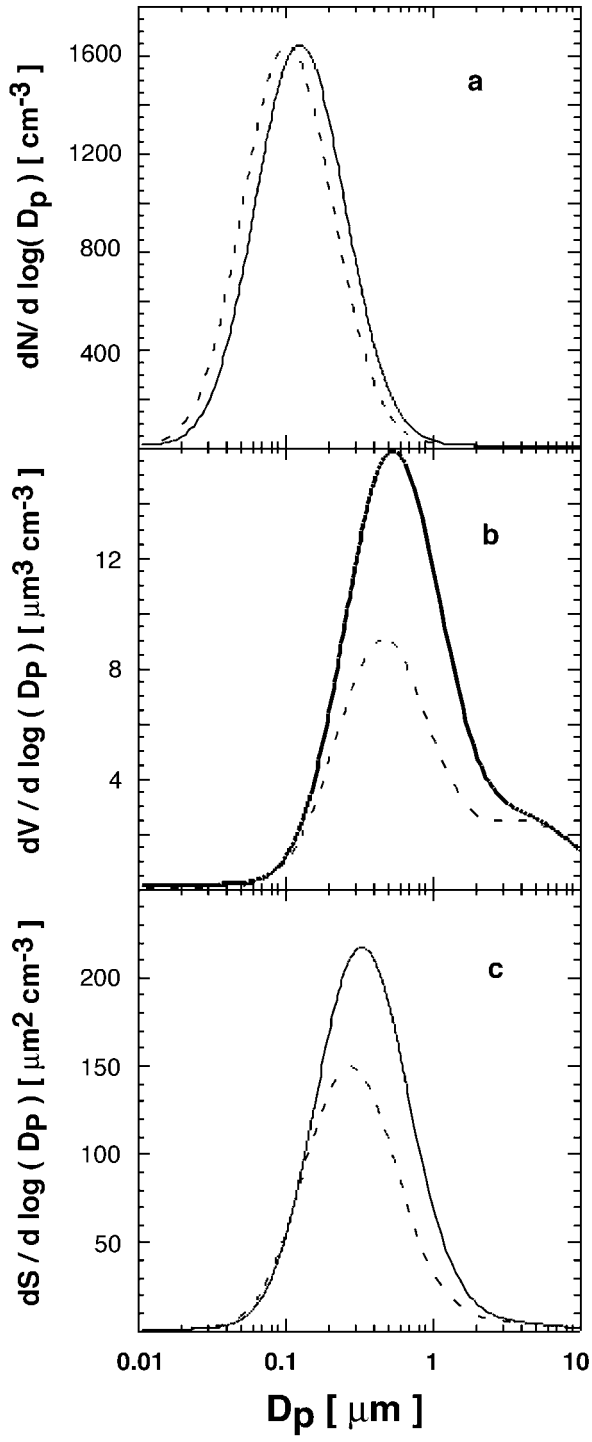

Figure 15. Size distribution at 17Z on July 13, 1995 for the GRSM1 grid cell. (a) Number concentration distribution, (b) volume concentration distribution, (c) surface area concentration distribution. The wet curves (solid) are for particles including aerosol water; the dry curves (dashed) are for the same particles without aerosol water.

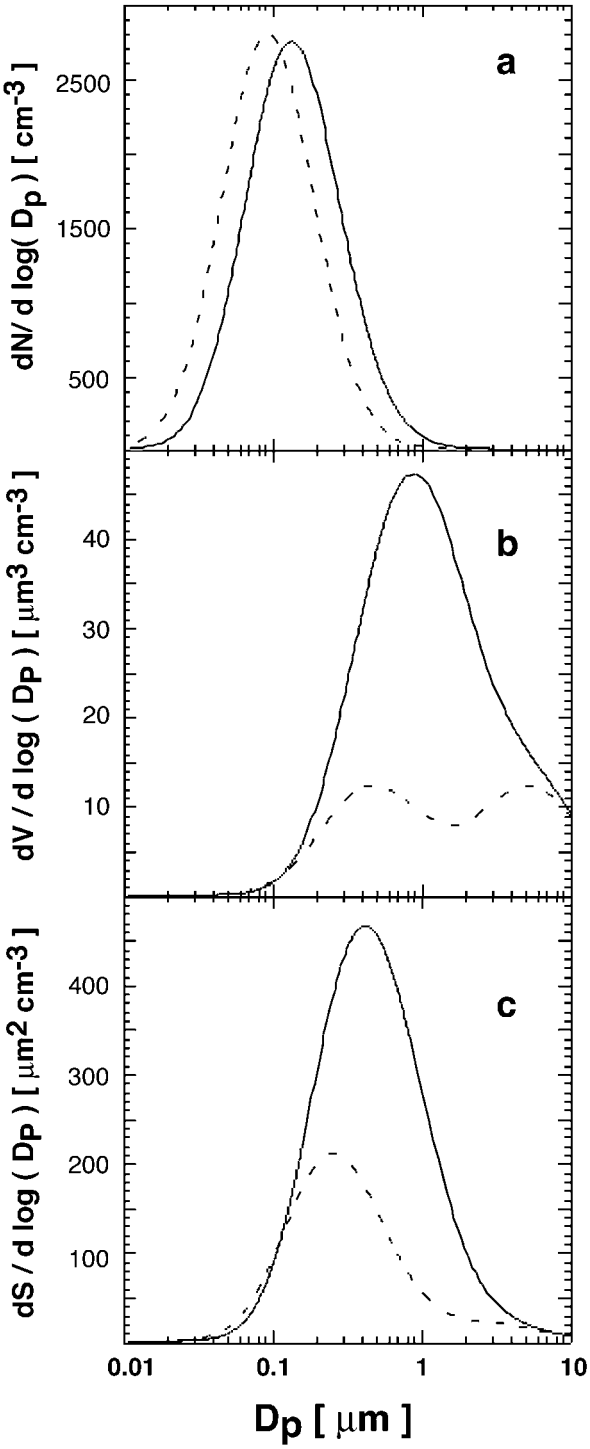

Figure 16. Size distribution at 17Z on July 13, 1995 for the WASH1 grid cell. (a) Number concentration distribution, (b) volume concentration distribution, (c) surface area concentration distribution. The wet curves (solid) are for particles including aerosol water; the dry curves (dashed) are for the same particles without aerosol water.

dimensional air quality model to produce reasonable results. A preliminary version of CMAQ using their method has been built and will become the operational version of CMAQ in a future release.

[56] *Kleeman et al.* [1997] have shown that various source types have size and species information that may be looked upon as a source signature. This assumes the availability of such source characteristics for the entire modeling domain. As noted in section 1.3, there are ongoing discussions with those responsible for the national emissions inventory. As more information becomes available, identification of source signatures may be possible for a larger domain than the Los Angeles area, and an effort similar to *Kleeman et al.* [1997], albeit using a modal approach, might be undertaken. Other improvements for primary particles are the inclusion of some chemical speciation for PM2.5 and PM10, using the new EPA emissions for 1996 and subsequent years. Work is under way for including marine aerosol, and a better treatment of fugitive dust.

[57] Future plans also include an intensive effort to evaluate the CMAQ aerosol component using atmospheric observations from selected field studies in which aerosol particles were observed. Comparison with routine visual range observations during the field study periods provides an additional method of evaluation, as shown by *Mebust et al.* [2003].

[58] **Acknowledgments.** The authors wish to thank Sonia M. Kreidenweis for her nucleation codes which have been incorporated within CMAQ. Grateful appreciation is extended to our supervisor Kenneth L. Schere for his support during the development of the aerosol component of CMAQ. Finally, we wish to thank Brian K Eder and Michelle R. Mebust for their comments and suggestions. This paper has been subjected to U.S. Environmental Protection Agency peer review and approved for publication. Mention of trade names or commercial products does not constitute endorsement or recommendation for use. Finally, the authors wish to thank the two anonymous reviewers for their valuable comments and suggestions.

References

Abramowitz, M., and I. A. Stegun, *Handbook of Mathematical Functions With Formulas, Graphs, and Mathematical Tables, Natl. Bur. Stand. Appl. Math. Ser.*, vol. 55, U.S. Govt. Print. Off., Washington, D.C., 1965.

Ackermann, I. J., H. Hass, M. Memmesheimer, A. Ebel, F. S. Binkowski, and U. Shanker, Modal aerosol dynamics model for Europe: Development and first applications, *Atmos. Environ.*, *32*, 2981–2999, 1998.

Binkowski, F. S., Aerosols in models-3 CMAQ, in *Science Algorithms of the EPA Models-3 Community Multiscale Air Quality (CMAQ) Modeling System*, chap. 10, *EPA/600/R-99/030*, Off. of Res. and Dev., U.S. Environ. Prot. Agency, Washington, D.C., 1999.

Binkowski, F. S., and U. Shankar, Development of an algorithm for the interaction of a distribution of aerosol particles with cloud water for use in a three-dimensional Eulerian air quality model, paper presented at the Fourth International Aerosol Conference, Los Angeles, Calif., 29 Aug. to 2 Sept. 1994.

Binkowski, F. S., and U. Shankar, The regional particulate model, 1, Model description and preliminary results, *J. Geophys. Res.*, *100*, 26,191–26,209, 1995.

Binkowski, F. S., S. M. Kreidenweis, D. Y. Harrington, and U. Shankar, Comparison of new particle formation mechanisms in the Regional Particulate Model, paper presented at the Fifteenth Annual Conference of the American Association for Aerosol Research, Orlando, Fla., 14–18 Oct. 1996.

Bower, K. N., and T. W. Choularton, A parameterisation of the effective radius of ice free clouds for use in global climate models, *Atmos. Res.*, *27*, 305–339, 1992.

Bowman, F. M., C. Pilinis, and J. H. Seinfeld, Ozone and aerosol productivity of reactive organics, *Atmos. Environ.*, *29*, 579–589, 1995.

Byun, D. W., and J. K. S. Ching, Science algorithms of the EPA Models-3 Community Multiscale Air Quality (CMAQ) modeling system, *EPA/600/R-99/030*, Off. of Res. and Dev., U.S. Environ. Prot. Agency, Washington, D. C., 1999.

Chang, J. S., R. A. Brost, I. S. A. Isaksen, S. Madronich, P. Middleton, W. R. Stockwell, and C. J. Walcek, A three-dimensional Eulerian acid deposition model: Physical concepts and formulation, *J. Geophys. Res.*, *92*, 14,681–14,700, 1987.

Chang, J. S., et al., The regional acid deposition model and engineering model, in*National Acid Precipitation Assessment Program, Acidic Deposition: State of Science and Technology*, vol. 1, *NAPAP SOS/T Rep. 4*, Natl. Acid Precip. Program, Washington, D.C., 1990.

Chaumerliac, N., Evaluation des Termes de Captation Dynamique dans un Modele Tridimensionel à Mesoechelle de Lessivage de L'Atmosphere, thesis, Univ. de Clermont II, U.E.R. de Rech. Sci. et Tech., 1984.

Davis, P. J., and P. Rabinowitz, *Numerical Integration*, Blaisdell, Waltham, Mass., 1967.

Evans, T. N., and G. R. Fournier, Simple approximation to extinction efficiency valid over all size ranges, *Appl. Opt.*, *29*, 4666–4670, 1990.

Fernández Díaz, J. M., M. A. Rodríguez Braña, B. Arganiza García, and P. J. García Nieto, A flux based characteristics method to solve particle condensational growth, *Atmos. Environ.*, *32*, 3027–3037, 1998.

Gelbard, F., Y. Tambour, and J. H. Seinfeld, Sectional representations for simulating aerosol dynamics, *J. Colloid Interface. Sci.*, *76*, 541–556, 1980.

Gery, M. W., G. Z. Whitten, J. P. Killus, and M. C. Dodge, A photochemical kinetics mechanism for urban and regional scale computer modeling, *J. Geophys. Res.*, *94*, 12,925–12,956, 1989.

Giauque, W. F., E. W. Hornung, J. E. Kunzler, and T. R. Rubin, The thermodynamics of aqueous sulfuric acid solutions and hydrates from 15 to 300 K, *J. Am. Chem. Soc.*, *82*, 62–67, 1960.

Harrington, D. Y., and S. M. Kreidenweis, Simulations of sulfate aerosol dynamics, I, Model description, *Atmos. Environ.*, *32*, 1691–1700, 1998a.

Harrington, D. Y., and S. M. Kreidenweis, Simulations of sulfate aerosol dynamics, part II, Model intercomparison, *Atmos. Environ.*, 1701–1709, 1998b.

Hatch, T., and S. P. Choate, Statistical description of the size properties of non-uniform particulate substances, *J. Franklin Inst.*, *207*, 1929.

Hildebrand, F. B., *Introduction to Numerical Analysis*, 2nd ed., McGraw-Hill, New York, 1974.

Hoffmann, T., C. D. O'Dowd, and J. H. Seinfeld, Iodine oxide homogeneous nucleation: An explanation for coastal new particle production, *Geophys. Res. Lett.*, *28*, 1949–1952, 2001.

Jacobson, M. Z., Development and application of a new air pollution modeling system, II, Aerosol module structure and design, *Atmos. Environ.*, *31*, 131–144, 1997.

Jacobson, M. Z., *Fundamentals of Atmospheric Modeling*, 656 pp., Cambridge Univ. Press, New York, 1999.

Kim, Y. P., J. H. Seinfeld, and P. Saxena, Atmospheric gas-aerosol equilibrium, I, Thermodynamic model, *Aerosol Sci. Technol.*, *19*, 157–181, 1993a.

Kim, Y. P., J. H. Seinfeld, and P. Saxena, Atmospheric gas-aerosol equilibrium, II, Analysis of common approximations and activity coefficient calculation methods, *Aerosol Sci. Technol.*, *19*, 182–198, 1993b.

Kleeman, M. J., G. R. Cass, and A. Eldering, Modeling the airborne particle complex as a source-oriented external mixture, *J. Geophys. Res.*, *102*, 21,355–21,372, 1997.

Korhonen, P., M. Kulmala, A. Laaksonen, Y. Viisanen, R. McGraw, and J. H. Seinfeld, Ternary nucleation of H_2SO_4, NH_3, and H_2O in the atmosphere, *J. Geophys. Res.*, *104*, 26,349–26,353, 1999.

Kulmala, M., A. Laaksonen, and L. Pirjola, Parameterization for sulfuric acid/water nucleation rates, *J. Geophys. Res.*, *103*, 8301–8307, 1998.

Kulmala, M., L. Pirjola, and J. M. Mäkalä, Stable sulphate clusters as a source of new atmospheric particles, *Nature*, *404*, 66–69, 2000.

Kulmala, M., M. Dal Maso, J. M. Mäkalä, L. Pirjola, M. Väkeva, P. Aalto, P. Miikkulainen, K. Hameri, and C. D. O'Dowd, On the formation, growth, and composition of nucleation mode particles, *Tellus, Ser. B*, *53*, 479–490, 2001.

Leaitch, W. R., Observations pertaining to the effect of chemical transformation in cloud on the anthropogenic aerosol size distribution, *Aerosol Sci. Technol.*, *25*, 157–173, 1996.

Mäkelä, J. M., I. K. Koponen, P. Aalto, and M. Kulmala, One-year data of submicron size modes of tropospheric background aerosol in southern Finland, *J. Aerosol Sci.*, *31*, 595–611, 2000.

Malm, W. C., Considerations in the measurements of visibility, *J. Air Pollut. Control Assoc.*, *29*, 1042–1052, 1979.

Malm, W. C., J. F. Sisler, D. Huffman, R. A. Eldred, and T. A. Cahill, Spatial and seasonal trends in particle concentration and optical extinction in the United States, *J. Geophys. Res.*, *99*, 1347–1370, 1994.

Mebust, M. R., B. K. Eder, F. S. Binkowski, and S. J. Roselle, Models-3 Community Multiscale Air Quality (CMAQ) model aerosol component, 2, Model evaluation, *J. Geophys. Res.*, *108*, doi:10.1029/2001JD001410, in press, 2003.

Meng, Z., D. Dabdub, and J. H. Seinfeld, Size-resolved and chemically resolved model of atmospheric aerosol dynamics, *J. Geophys. Res.*, *103*, 3419–3435, 1998.

Mozurkewich, M., The dissociation constant of ammonium nitrate and its dependence on temperature, relative humidity, and particle size, *Atmos. Environ., Part A*, *27*, 261–270, 1993.

Nair, P. V. N., and K. G. Vohra, Growth of aqueous sulphuric acid droplets as a function of relative humidity, *J. Aerosol Sci.*, *6*, 265–271, 1975.

Odum, J. R., T. Hoffman, F. Bowman, D. Collins, R. C. Flagan, and J. H. Seinfeld, Gas/particle partitioning and secondary organic aerosol yields, *Environ. Sci. Technol.*, *30*, 2580–2585, 1996.

Pandis, S. N., R. A. Harley, G. R. Cass, and J. H. Seinfeld, Secondary organic aerosol formation and transport, *Atmos. Environ., Part A*, *26*, 2269–2282, 1992.

Pankow, J. F., An absorption model of gas/particle partitioning of organic compounds in the atmosphere, *Atmos. Environ.*, *28*, 185–188, 1994a.

Pankow, J. F., An absorption model of gas/particle partitioning involved in the formation of secondary organic aerosol, *Atmos. Environ.*, *28*, 189–193, 1994b.

Pirjola, L., A. Laaksonsen, P. Aalto, and M. Kulmala, Sulfate aerosol formation in the Arctic boundary layer, *J. Geophys. Res.*, *103*, 8309–8321, 1998.

Pitchford, M. L., and W. C. Malm, Development and applications of a standard visual index, *Atmos. Environ.*, *28*, 1049–1054, 1994.

Pruppacher, H. R., and J. D. Klett, *Microphysics of Clouds and Precipitation*, D. Reidel, Norwell, Mass., 1978.

Saxena, P., and L. Hildemann, Water-soluble organics in atmospheric particles: A critical review of the literature and application of thermodynamics to identify candidate compounds, *J. Atmos. Chem.*, *24*, 57–109, 1996.

Saxena, P., L. M. Hildemann, P. H. McMurry, and J. H. Seinfeld, Organics alter hygroscopic behavior of atmospheric particles, *J. Geophys. Res.*, *100*, 18,755–18,770, 1995.

Schell, B., I. J. Ackermann, H. Hass, F. S. Binkowski, and A. Ebel, Modeling the formation of secondary organic aerosol within a comprehensive air quality modeling system, *J. Geophys. Res.*, *106*, 28,275–28,293, 2001.

Seigneur, C., A. B. Hudischewskyj, J. H. Seinfeld, K. T. Whitby, E. R. Whitby, J. R. Brock, and H. M. Barnes, Simulation of aerosol dynamics: A comparative review of mathematical models, *Aerosol Sci. Technol.*, *5*, 205–222, 1986.

Seinfeld, J. H., and S. N. Pandis, *Atmospheric Chemistry and Physics From Air Pollution to Climatic Change*, John Wiley, New York, 1998.

Shankar, U., and F. S. Binkowski, Sulfate aerosol wet deposition in a three-dimensional Eulerian air quality modeling framework, paper presented at the Fourth International Aerosol Conference, Los Angeles, Calif., 29 Aug. to 2 Sept. 1994.

Slinn, W. G. N., Rate-limiting aspects of in-cloud scavenging, *J. Atmos. Sci.*, *31*, 1172–1173, 1974.

Spann, J. F., and C. B. Richardson, Measurement of the water cycle in mixed ammonium acid sulfate particles, *Atmos. Environ.*, *19*, 825–919, 1985.

Tang, I. N., and H. R. Munkelwitz, Water activities, densities, and refractive indices of aqueous sulfates and sodium nitrate droplets of atmospheric importance, *J. Geophys. Res.*, *99*, 18,801–18,808, 1994.

Walcek, C. J., and G. R. Taylor, A theoretical method for computing vertical distributions of acidity and sulfate production within cumulus clouds, *J. Atmos. Sci.*, *43*, 439–455, 1986.

Weber, R. J., J. J. Marti, P. H. McMurry, F. L. Eisele, D. J. Tanner, and A. Jefferson, Measurements of new particle formation and ultrafine particle growth rates at a clean continental site, *J. Geophys. Res.*, *102*, 4375–4385, 1997.

Wexler, A. S., F. W. Lurmann, and J. H. Seinfeld, Modeling urban and regional aerosols, I, Model development, *Atmos. Envion.*, *28*, 531–546, 1994.

Whitby, E. R., and P. H. McMurry, Modal aerosol dynamics modeling, *Aerosol Sci. Technol.*, *27*, 673–688, 1997.

Whitby, E. R., P. H. McMurry, U. Shankar, and F. S. Binkowski, Modal aerosol dynamics modeling, *Rep. 600/3-91/020*, Atmos. Res. and Exposure Assess. Lab., U.S. Environ. Prot. Agency, Research Triangle Park, N. C., 1991. (Available as *PB91-161729/AS* from Natl. Tech. Inf. Serv., Springfield, Va.).

Whitby, K. T., The physical characteristics of sulfur aerosols, *Atmos. Environ.*, *12*, 135–159, 1978.

Willeke, K., and J. E. Brockmann, Extinction coefficients for multimodal atmospheric particle size distributions, *Atmos. Environ.*, *11*, 995–999, 1977.

Wright, D. L., R. McGraw, C. M. Benkovitz, and S. E. Schwartz, Six-moment representation for multiple aerosol populations in a sub-hemi-

spheric chemical transformation model, *Geophys. Res. Lett.*, *27*, 967–970, 2000.

Yu, F., and R. P. Turco, From molecular clusters to nanoparticles: Role of ambient ionization in tropospheric aerosol formation, *J. Geophys. Res.*, *106*, 4797–4814, 2001.

Zhang, Y., C. Seigneur, J. H. Seinfeld, M. Z. Jacobson, and F. S. Binkowski, Simulation of aerosol dynamics: A comparative review of algorithms used in air quality models, *Aerosol Sci. Technol.*, *31*, 487–514, 1999.

Zhang, Y., C. Seigneur, J. H. Seinfeld, M. Z. Jacobson, S. L. Clegg, and F. S. Binkowski, A comparative review of inorganic aerosol thermodynamics equilibrium modules: Differences and their likely causes, *Atmos. Environ.*, *34*, 117–137, 2000.

F. S. Binkowski, 717 Tinkerbell Road, Chapel Hill, NC 2717-3013, USA. (frank_binkowski@unc.edu)

S. J. Roselle, National Exposure Research Laboratory, U.S. EPA, MD 80, Research Triangle Park, NC 27711, USA.